Article

Mechanistic Insights into Enantioselective Gold-Catalyzed Allylation of Indoles with Alcohols: the Counterion Effect

Marco Bandini, Andrea Bottoni, Michel Chiarucci, Gianpiero Cera, and Gian Pietro Miscione

J. Am. Chem. Soc., **Just Accepted Manuscript** • DOI: 10.1021/ja3086774 • Publication Date (Web): 30 Nov 2012

Mechanistic Insights into Enantioselective Gold-Catalyzed Allylation of Indoles with Alcohols: the Counterion Effect

Marco Bandini,* Andrea Bottoni, Michel Chiarucci, Gianpiero Cera, Gian Pietro Miscione*

Dipartimento di Chimica "G. Ciamician", Alma Mater Studiorum – Università di Bologna, via Selmi 2, 40126 Bologna, Italy.

KEYWORDS Alcohols, Asymmetric Catalysis, Catalytic Mechanism, Counterions, Computational Investigation, Gold, Indole.

Supporting Information Placeholder

ABSTRACT: Enantioselective gold-catalysis is emerging as a powerful tool in organic synthesis for the stereoselective manipulation of unfunctionalized unsaturated hydrocarbons. Despite the exponential growth, the molecular complexity of common chiral gold complexes generally prevents a complete description of the mechanism steps and activation modes being documented. In this study, we present the results of a combined experimental-computational (DFT) investigation of the mechanism of the enantioselective gold-catalyzed allylic alkylation of indoles with alcohols. A step-wise S_N2'-process (*i.e. anti*-auroindolination of the olefin, proton-transfer and subsequent *anti*-elimination [Au]-OH) is disclosed, leading to a library of tricyclic-fused indole derivatives. The pivotal role played by the gold counterion, in terms of molecular arrangement (*i.e. "folding effect*") and proton-shuttling in restoring the catalytic species, is finally documented.

INTRODUCTION

Over the recent years, enantioselective [gold(I)] catalysis has become a concrete reality in the realm of asymmetric synthesis.[1] The "re-discovering" of this coinage metal in homogeneous catalysis allowed to expand significantly the current synthetic portfolio for the selective manipulation of unactivated unsaturated hydrocarbons. Moreover, a concrete contribution toward the replacement of "old" chemistry with more efficient and sustainable chemical methodologies was documented.[2] Worth noting is the concomitant and rapid diffusion of enantioselective gold catalysis in organic synthesis, that can be also ascribable to the current large volume of synthetically flexible and sterically congested P- and NCH-based chiral ligands capable of generating stable and fine-tunable chiral gold complexes. In particular, chiral C*1*-symmetric mononuclear, C*2*-symmetric binuclear and C*3*-symmetric trinuclear[3] gold(I) systems have already shown particular pertinence in the stereoselective manipulation of unactivated π-systems.[1b]

Despite efficiency, the unambiguous elucidation of reaction intermediates in gold catalysis still remains a challenging task,[4] and even more pronounced are the mechanistic ambiguities within enantioselective gold-catalyzed processes. The state of the art is partly ascribable to the complex architectures of the chiral [Au(I)] π-acids used in asymmetric transformations. In particular, binuclear gold complexes of general formula [P-P(AuX)$_2$][5] lead to the possibility of multiple reaction pathways/activation modes, but restrict at the same time the applicability of experimental/computational treatments. Furthermore, additional issues in mechanism elucidation lie in the mandatory activation of the chiral gold chloride pre-catalysts with silver-salts (*i.e.* halide scavengers)[6] in order to ensure satisfying levels of carbophilicity.[7] In this context the catalytic performance of the resulting [P-P(AuX)$_2$] adducts (X: SbF_6, OTf, BF_4, OBz, NTf_2, ClO_4, etc.) turns out to be remarkably affected by the counterion utilized and, with the exception of a few leading examples,[8] the real role of the anions over both kinetic and stereochemical reaction profiles still remains obscure.[9]

In line with our ongoing interests on the heterocyclic-oriented methodology development,[10] some of us have recently reported on the use of cationic chiral binuclear [Au(I)] complexes as efficient electrophilic activators of unfunctionalized carbon-carbon double bonds towards the intramolecular allylic functionalization of indoles.[11] In particular, environmentally benign allylic alcohols were employed in additive-free enantioselective nucleophilic substitution reactions (Figure 1).[12]

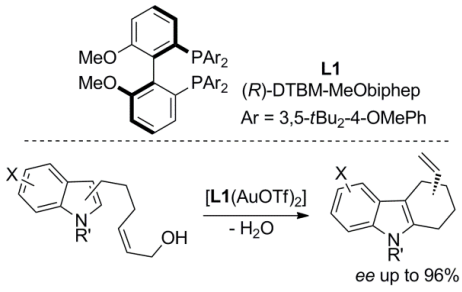

Figure 1. Gold-catalyzed enantioselective allylic alkylation of indoles with primary alcohols.

The intramolecular methodology worked smoothly for both C(2)- and C(3)-alkylation of indolyl cores, several tethering units as well as functional groups were also well tolerated delivering a rapid route to key building blocks for biologically active alkaloids.[13] In particular, a range of 1-vinyl- (**2**), 4-vinyl-tetrahydrocarbazoles (**4**) and 4-vinyl-tetrahydro-β-carbolines (**3**, vinyl-THBCs) were isolated in good yields and excellent enantiomeric ratios (Chart 1). Moreover, the meth-

odology found application also in the enantioselective synthesis of 1-vinyl-morpholines via intramolecular dehydrating oxa-allylic alkylation with diols [12c]

CHART 1. A representative collection of tricyclic indolyl scaffolds available through the intramolecular enantioselective allylic alkylation procedure (in red the newly formed C-C bonds, with (*R*)-DTBM-MeObiphep, toluene, 0 °C/rt, 16 h).

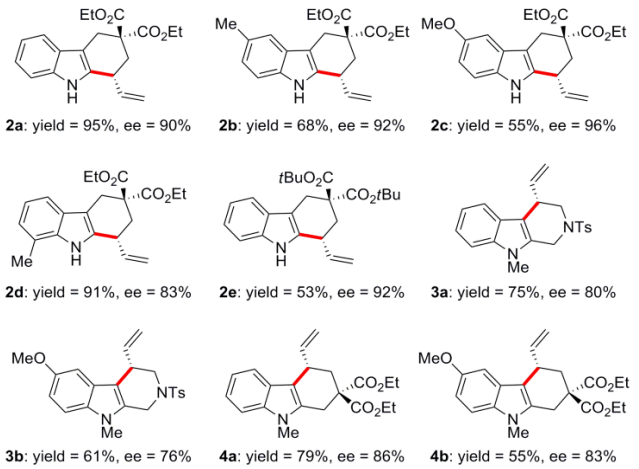

Preliminary experimental evidences suggested that some specific structural features of the acyclic precursors and gold-pre-catalysts, namely: i) configuration of the carbon-carbon double bond, ii) nature of the gold-counterion and iii) leaving hydroxyl group played a pivotal role over the chemical and optical outcome of the process.[12a] These aspects open up intriguing mechanistic perspectives concerning the coordination mode of the binuclear gold species with the allylic alcohols (*i.e.* single site- *vs* bidentate interaction) and lead us to envisage the presence of a complex interplay of secondary interactions involving the counterion during the enantiodiscriminating step of the reaction. Moreover, important issues concerning the mechanistic course are still unsolved. Firstly, both S_N1 and S_N2' (stepwise or concerted) reaction channels constitute reasonable mechanistic alternatives to rationalize the overall chemical output (Figure 2). Secondly, the regiochemistry of the initial nucleophilic attack of the indole core on the alkylating agent (*i.e* C(2) *vs* C(3) position) is still matter of debate.

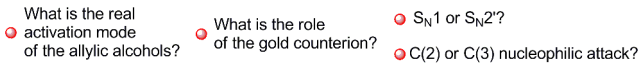

Figure 2. Still open tasks in the mechanistic description of the gold-catalyzed allylic alkylation of indoles with alcohols.

In this investigation, we wish to elucidate these intriguing and still pending problems, by documenting a combined experimental and theoretical investigation in which, the enantioselective synthesis of 1-vinyl-tetrahydrocarbazoles **2**, was used as the model-reaction.[14]

RESULTS AND DISCUSSION

Gold-catalyzed organic manipulations of π-systems commonly deal with a pronounced reagent-controlled stereoselectivity.[15,16] Some exceptions concern the dehydrative nucleophilic substitutions[17] with enantioenriched π-alcohols as alkylating agents in which the starting material undergoes partial or total racemization.[18]

Recent reports by Widenhoefer[15a,g,i] and Aponick[15c,f] on the [Au(I)]-assisted nucleophilic allylic substitution with alcohols, have further pointed out the influence of stereochemistry of the reaction partners on the entire process. However, despite these inspiring records, reagent-controlled stereochemistry in gold-promoted *enantioselective* allylic alkylation reactions still remains barely investigated.[15j,19]

In our original communication,[12a] we discussed on the highly stereoselective synthesis of 1-vinyl-tetrahydrocarbazole (*R*)-**2a** (yield = 95%, *ee* = 90%), by subjecting the corresponding acyclic precursor (*Z*)-**1a** to the dehydrative ring-closing allylic alkylation, in the presence of (*R*)-DTBM-MeObiphep$(AuCl)_2$/AgOTf (10 mol%, in toluene at 0 °C, Scheme 1). On the contrary, the diastereomeric alcohol (*E*)-**1a** proved to be completely inert under best reaction conditions.

SCHEME 1. Proofs of reagent-controlled stereochemistry in the synthesis of 1-vinyl-tetrhydrocabazole **2a**.

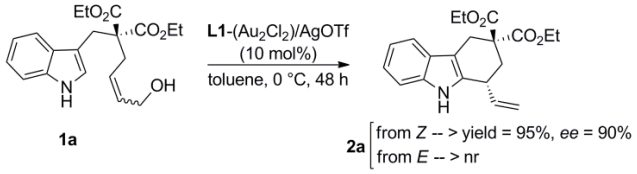

At first instance, the recorded dichotomy in reactivity could be rationalized in terms of an unfavorable spatial arrangement of the sterically demanding chiral bimetallic catalyst with the *trans* allylic alcohol. However, no further information was available.

Moreover, the pivotal role of the counterion in affecting the reaction profile, was demonstrated by screening a range of silver salts in the model reaction ((*Z*)-**1a** → **2a**). The results are collected in Table 1.

TABLE 1. Counterion effect in the gold-catalyzed enantioselective synthesis of tetrahydrocarbazole **2a**.[a]

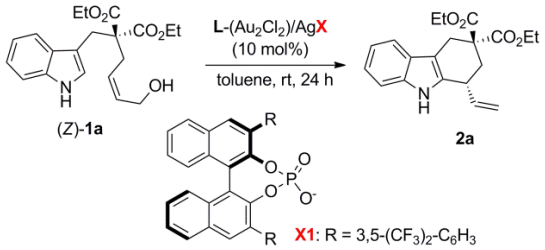

Entry	L	AgX	Yield (%)[b]	Ee (%)[c]
1	**L1**	$AgBF_4$	55	87
2	"	$AgSbF_6$	75	62
3	"	$AgNTf_2$	95	65

4	"	AgOTf	78	88
5	"	AgOTs	10	92
6	"	AgOPNB	traces	nd
7	"	Ag**X1**	traces	nd
8	dppm	Ag**X1**	traces	nd

[a] All reactions were carried out under nitrogen atmosphere with anhydrous toluene, unless otherwise specified. [b] Isolated yields after flash chromatography. [c] Determined by HPLC analysis with chiral column. nd = not determined.

Generally, moderate to high enantiomeric excesses were recorded with fluoro-based counterions (entries 1-4, 62-88%). Excellent stereoinduction was also obtained in the presence of AgOTs (*ee* = 92%, entry 5) albeit along with modest yield. Here, the lower turnovers observed for AgOTs and AgOPNB (PNB: *p*-nitrobenzoate, entry 6)[20] can be rationalized in terms of the higher coordinating character of these anions towards [Au(I)] atoms with respect to triflate and hexafluoroantimonate. Finally, the pertinence of the chiral counterion strategy,[8b,21] in our ring-closing protocol was assessed in the presence of both chiral [**L1**(Au_2Cl_2)] and achiral [dppm(Au_2Cl_2)] gold complexes and chiral silver salt Ag**X1** (entries 7-8). However, the desired tetracyclic scaffold was formed only in traces.

Therefore, beside the expected role of the counterion on the kinetic reaction profile, we can first conclude that the anions must be involved in some of the key-intermediates which are responsible for the stereochemical translation.

To elucidate the above described points (in particular reagent-controlled stereochemistry and counterion effect) we have carried out a computational investigation of the reaction mechanism using a DFT approach and two different model-systems differing in the size of the ligand coordinating the two gold atoms. The basic framework of the system is formed by compound **1a** (where we have replaced the two CO_2Et groups on the side-chain with two hydrogen atoms) and the gold complex **L1**$(AuOTf)_2$. In the smaller system (**MODEL 1**) Ar is a simple benzene ring while in the larger system (**MODEL 2**) Ar = 3,5-(*t*-Bu)$_2$-4-OMe-Ph.

In order to verify the reliability of our computational models we firstly investigated experimentally the role of the malonyl tethering unit. To this aim, alcohol (*Z*)-**1f** proved to be synthetically accessible in five steps starting from indolyl-alcohol **5** (Scheme 2, unoptimized yields are reported). Interestingly, by subjecting (*Z*)-**1f** to optimal conditions, a prolonged reaction time (48 h, yield = 58%) was required, with respect to model substrates (**1a-e**), supporting the presence of a Thorpe-Ingold effect[22] played by the malonyl group. However, satisfying enantiocontrol was still produced (*ee* = 70%), underlying the reliability of our model-system.

SCHEME 2. Proving the role of the malonyl groups in the enantioselective ring-closing process.

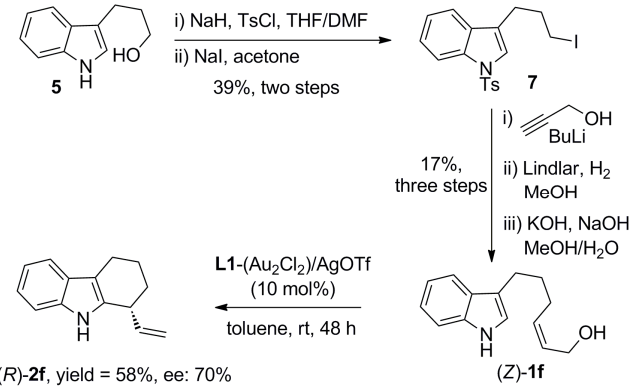

The small model-system. We discuss first the results obtained for **MODEL 1**. A schematic representation of two possible low energy structures of the starting reactants is given in Figure 3. A point concerning Figure 3A and 3C should be stressed. Since in these figures we have adopted a two-dimensional representation, several atomic distances are not realistic and appear much longer (or shorter) than in the real molecules. Also, the labels used to identify the various atoms do not follow the order usually employed for aromatic rings. Furthermore, within the carbon framework we have explicitly indicated only the hydrogen atoms needed to identify the stereochemical features of the process. A more realistic three-dimensional picture of the model-system is given in Figure 3B and 3D.

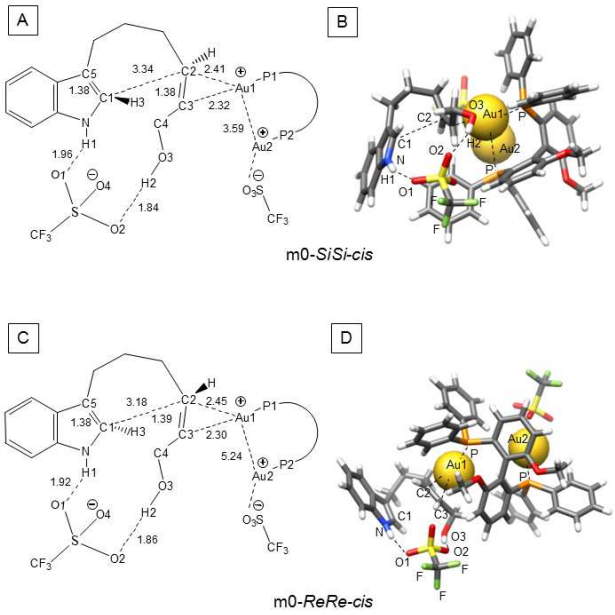

Figure 3. Two-dimensional and three-dimensional representations of **m0-*SiSi-cis*** and **m0-*ReRe-cis*** (bond lengths are in Ångstroms).

In these molecules each gold atom has a formal positive charge +1, while each triflate group bears a negative charge; therefore the total charge is zero. The initial gold complex (reactants) can exist as different isomers. Some of them are conformational isomers that mainly differ in the relative position of the two reacting moieties (indole and allylic alcohol group) and in the nature of triflate-substrate interactions. Further

structural arrangements originate from the *trans-cis* configuration of the C2-C3 double bond.

The energies of the various isomeric forms of the starting reactant species are reported in the upper side (A) of the diagram of Figure 4. To denote the various complexes we have adopted appropriate names that contain information concerning the indole and alkene faces (*Re* or *Si*) involved in the reaction and the configuration of the C2-C3 double bond. Thus, for instance, **m0-*SiSi-cis*** indicates that the C2-C3 double bond has a *cis* configuration and the reaction involves the two *Si* faces of the indole moiety and olefin C2-C3 fragment. In Figure 4A we have collected the energy levels of the *cis* isomers on the left and those of the *trans* isomers on the right. **m0-*SiSi-cis*** is the most stable isomer and corresponds to the structure depicted in Figure 3A and 3B where it is easy to recognize the strong η^2 interaction between the double bond C2-C3 and one (Au1) of the two gold atoms. This interaction is not symmetrical, the Au1-C3 bond length (2.32 Å) being shorter than Au1-C2 (2.41 Å). Interestingly, in this structure one triflate ion is bridging the indole hydrogen H1 and the hydroxyl oxygen O3 by means of two rather strong hydrogen-bonds: NH1···O1 (H1···O1 = 1.96 Å) and O3H2···O2 (H2···O2 = 1.84 Å). In the following discussion we shall refer to this bridging interaction as the "*folding effect"* or *"chelating effect"* of the anion since it forces the two reactive sites of the molecule to move closer adopting the right orientation to react. As a consequence the **m0-*SiSi-cis*** complex assumes a U-turn-type geometry, as evidenced in Figure 3A and B, where the C1···C2 distance is 3.34 Å. The other triflate ion is bonded to the second gold atom Au2. This atom does not interact with the C2-C3 double bond and we shall see that it behaves like a "spectator" throughout the entire process. The computed Mulliken charges reveal that, even if both C2 and C3 are negative, the former (which is subjected to the nucleophilic attack) is less negative than the latter (net charges are -0.16 and -0.35, respectively).

The diagram of Figure 4A shows that the isomers where the *Re* face of the indole moiety (carbon C1) is involved in the reaction *i.e.* **m0-*ReRe-cis*** and **m0-*ReSi-cis*** are higher in energy: 2.4 and 3.1 kcal mol^{-1} above **m0-*SiSi-cis***, respectively. The structural features of **m0-*ReRe-cis*** (see Figure 3C and 3D) are similar to those of **m0-*SiSi-cis*,** except for a larger Au1-Au2 distance: 5.24 Å instead of 3.59 Å. Although well below the sum of the van del Waals radii (3.80 Å), Au-Au distances greater than 3.50 Å are only marginally ascribed to aurophilic interactions.[23] However, a contribution of this kind cannot be completely ruled out in our system to account for the slight energy difference between the **m0-*ReRe-cis*** and **m0-*SiSi-cis*** isomers. The triflate ion exerts here the same "folding effect" previously described. This effect seems to be more important in **m0-*ReRe-cis*** since the C1···C2 distance is shorter (3.18 Å) with respect to **m0-*SiSi-cis***.

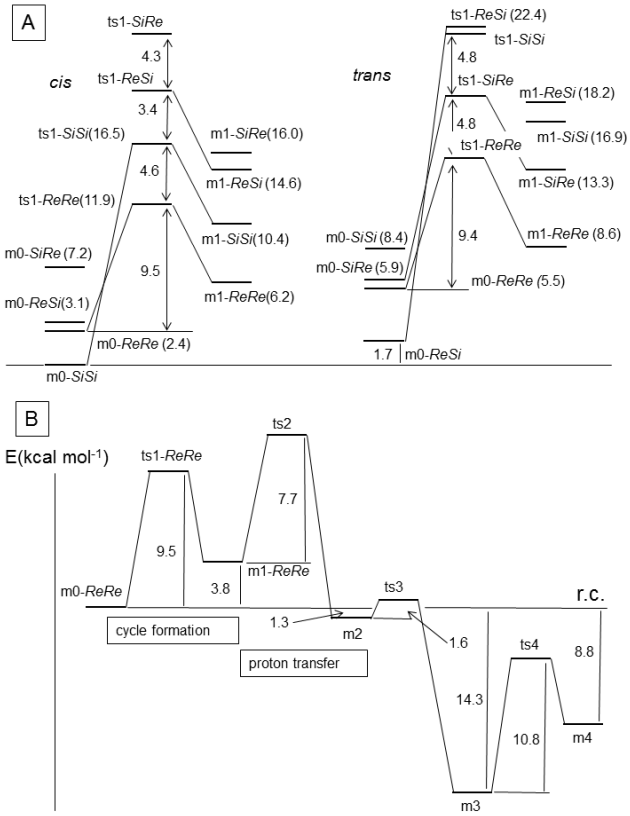

Figure 4. (A) Energies of the *cis* (left) and *trans* (right) starting adducts **m0** in the various conformations, the corresponding transition states **ts1** and the resulting intermediates **m1** (**MODEL 1)**. Values in parenthesis are relative to **m0-*SiSi-cis***. (B) Energy profile for the reaction path originating from **m0-*ReRe-cis.*** Energies in kcal mol^{-1}.

Starting adducts featuring a *trans* C2-C3 double bond have also been considered. Even if the overall bonding pattern of these structures is similar to that of the corresponding *cis* species, the energy spectrum significantly varies (see right side of Figure 4A): **m0-*ReSi-trans*** is now the most stable isomer (only 1.7 kcal mol^{-1} above **m0-*SiSi-cis***), while the two isomers where the reaction occurs on the *Re* face of the C2-C3 olefin fragment, **m0-*ReRe-trans*** and **m0-*SiRe-trans***, are 5.5 and 5.9 kcal mol^{-1} higher than **m0-*SiSi-cis***, respectively. The highest energy structure becomes **m0-*SiSi-trans***, 8.4 kcal mol^{-1} above **m0-*SiSi-cis*** (a two-dimensional representation of **m0-*ReRe-trans*** is given in Figure S1 of the Supporting Information). Since the energies of the *cis* and *trans* structures are not so far one from the other and the approximations adopted in the simpler model-system could seriously affect the energy spectrum, all species have been initially considered as possible starting complexes of alternative reaction channels.

Our computations have shown the possibility of a different coordination mode involving the gold atoms and the allyl OH group. This alternative molecular arrangement is characterized by a 7-membered ring that includes Au1, Au2, O4, H2, O3, C4, C3 and can be observed when the allylic hydroxyl points towards the Au2 atom and the second triflate group. However, these molecular aggregates (deriving from the two-

site binding coordination mode) resulted quite unstable, lying about 10 kcal mol^{-1} above **m0-*SiSi-cis*** regardless of their configuration. Also, they originate very high reaction pathways. For these reasons they will not be considered in the following discussion.

The preliminary computational studies pointed to the above mentioned "*folding effect"* (played by the triflate counterion as shown in **m0-*SiSi-cis*** and **m0-*ReRe-cis***), favoring the best relative orientation of the C1 and C2 atoms to form the new C-C bond. This effect should directly involve only one gold atom of the binuclear catalyst in the electrophilic activation of the olefin bond (single-site coordination).

Seeking for experimental evidence to support this hypothesis, we investigated modified systems characterized by the impossibility of establishing the above mentioned network of H-bonds responsible for the *"folding effect"*. Following our mechanistic model, this impossibility should cause a decrease of chemical yield and stereoinduction. Thus, indole-alcohols carrying either the *N*(1)-substituted indole rings ((*Z*)-**1g,h**) or the *O*Me group in place of the allyl OH (**1i)** were prepared and reacted under optimal conditions (Scheme 3). Interestingly, while no conversion was observed for *N*(1)-Me (**1g**) and methylether **1i**, *N*(1)-allyl compound **1h** yielded **2h** in 22% yield but in racemic form. All these experimental evidences support the idea that hydrogen interactions (as shown in Figure 3) play an essential role both in the rate limiting and stereo-differentiating steps of the reaction (*vide infra* for mechanistic details).

SCHEME 3. Denying the establishment of hydrogen interactions *via* the acid *N*1(H) and OH protons. Both reaction rate and stereoselection are markedly eroded.

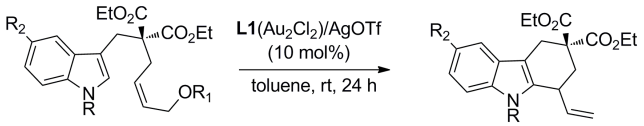

(*Z*)-**1g**: R = Me, R_1 = R_2 =H
(*Z*)-**1h**: R = allyl, R_1 = R_2 =H
(*Z*)-**1i**: R = H, R_1 = Me, R_2 = Br

2g,i: yield = traces
2h: yield = 22%; ee = 0%

The knowledge of the optimized reagent structures, together with the above described experimental results, has made possible to envisage a reasonable mechanistic scheme. Because of the single-site coordination of the cationic gold complex and relative low oxophilicity, the formation of allylic carbocation intermediates (required by a S_N1-type mechanism) seems unlikely. A S_N2' mechanism represents a more feasible hypothesis, albeit ambiguity between concerted and step-wise profiles remains unsolved.

First reaction step: outer-sphere carboauration of the C-C double bond. In the first reaction step the indole C1 carbon attacks the C2 olefin carbon, affording a new C1-C2 bond and a six-membered cycle. This event is triggered by the electrophilic activation of the olefin played by the gold catalyst, with some important consequences: (i) the loss of aromaticity of the pyrrole ring; (ii) the formation of a formally covalent σ Au1-C3 bond; (iii) the transfer of the formal positive charge from Au1 to C5; (iv) the formation of three new stereocenters (C1, C2 and C3).

ts1-*ReRe-cis* is the most stable transition state located for the first reaction step in which the new C1-C2 bond is forming (the C1-C2 distance is 2.05 Å). A schematic representation of **ts1-*ReRe-cis*** is given in Figure 5. The structural changes occurring in this step are clearly evidenced by the values of the geometrical parameters: since C2-C3 is turning into a single bond, its lengths is greater (1.46 Å) with respect to reactants. According to the formation of a Au1-C3 σ bond, the asymmetry featuring the interaction between Au1 and the C2 and C3 atoms becomes more pronounced (the Au1-C3 and Au1-C2 distances are 2.17 and 2.90 Å, respectively). Furthermore, a strengthening of the hydrogen-bond between the indolic hydrogen H1 and the triflate oxygen O1 is observed (H1···O1 = 1.78 Å; it was 1.92 Å in **m0-*ReRe-cis***) as a consequence of the negative charge displacement from the indole ring toward C2, which increases the H1 acidity. The computed energy barrier for **ts1-*ReRe-cis*** is rather low (only 9.5 kcal mol^{-1}). This can be explained by the π-acidity of Au1, which enhances the electrophilicity of C2 and the pronounced "*folding effect*" of the triflate ion forcing C1 and C2 to the best relative position for the attack.

Unlike what found for the starting reactants for which the three most stable isomers are rather close in energy (within a range of 3.1 kcal mol^{-1}), **ts1-*ReRe-cis*** turns out to be highly favored over the other possible transition structures originating from the various *cis* starting adducts. To have an exhaustive picture of the energetics of the various reaction pathways, we have reported in Figure 4A the energy levels of all possible transitions states (originating from the different isomeric **m0** species) and the resulting **m1** intermediates. In particular, the transition state **ts1-*SiSi-cis*** stemming from the most stable isomer **m0-*SiSi-cis***, lies 4.6 kcal mol^{-1} above **ts1-*ReRe-cis*** and is characterized by a much larger intrinsic energy barrier (16.5 kcal mol^{-1}). Thus, it cannot compete with **ts1-*ReRe-cis***. It is interesting to note that the two hydrogen-bonds involving the triflate fragment *i.e.* H1···O1 and H2···O2, are weaker in **ts1-*SiSi-cis*** with respect to **ts1-*ReRe-cis*** (the corresponding distances are 1.82 Å and 1.89 Å, respectively). Higher energy values feature the two additional *cis* transition states **ts1-*ReSi-cis*** and **ts1-*SiRe-cis***.

The only reaction channel which, in principle, could compete with **m0-*ReRe-cis*** → **ts1-*ReRe-cis*** is that associated with **ts1-*ReRe-trans***, whose structural features are similar to those of **ts1-*ReRe-cis*** except for the reversed configuration of the C2-C3 double bond (a two-dimensional representation of **ts1-*ReRe-trans*** is given in Figure S1). It is interesting to examine in this case the mechanism of the *"folding effect"* exerted by the triflate ion. Because of the *trans* configuration of the C2-C3 double bond, the triflate oxygen O2 forms a strong H-bond with the allylic hydroxyl (O3H2···O2 = 1.77 Å), while the triflate O1 is too far away to interact simultaneously with the indole NH1 bond, as observed in the *cis* structure. However, since the H2···O2 interaction makes O3 basic enough to establish a hydrogen bond with the indole ring (NH1···O2 = 1.81 Å), the triflate "*folding effect"* is still effective.

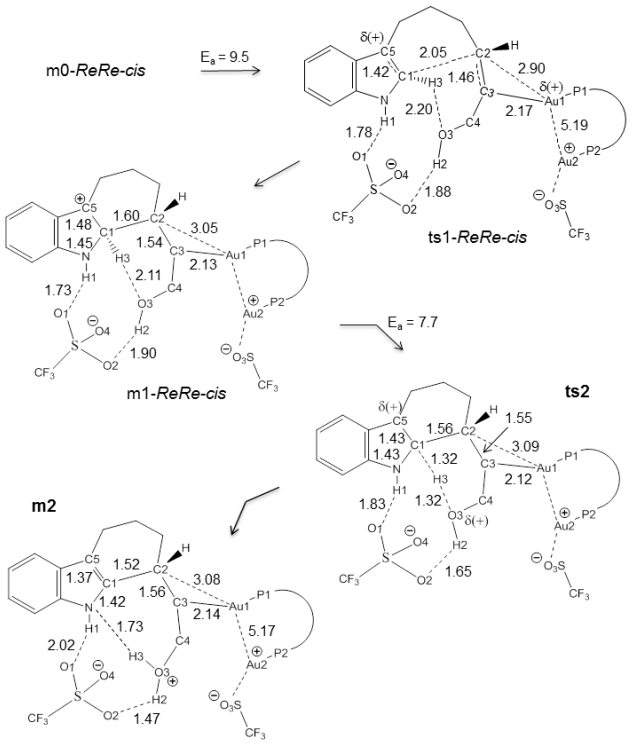

Figure 5. Two-dimensional representations of the critical points **ts1**, **m1**, **ts2** and **m2** located along the reaction path originating from **m0-*ReRe-cis*** (bond lengths are in Ångstroms).

A comparison between the *cis* and *trans* structures shows that in both cases the most stable starting adducts (**m0-*SiSi-cis*** and **m0-*ReSi-trans***) do not originate the most likely reaction paths (in particular, for the *trans* structure the intrinsic activation barrier for **m0-*ReSi-trans*** is very high *i.e.* 23.1 kcal mol^{-1}). Thus, for both *cis* and *trans* configuration the "active" species does not corresponds to the most populated one and an equilibrium must exist between this conformation and the actually "active" conformation. Since the energy difference between these two conformational isomers is lower in the *cis* case (2.4 kcal mol^{-1}) than in *trans* case (3.8 kcal mol^{-1}, see Figure S1) and the intrinsic activation barrier is almost identical in the two cases (9.5 and 9.4 kcal mol^{-1}), the simpler model-system seems to suggest that both *cis* and *trans* adducts should be reactive, but that the former should react faster than the latter. Since all remaining *trans* transition structures are much higher in energy, the corresponding reaction channels can be immediately discarded.

Before considering a more complex and realistic model-system (**MODEL 2**), to obtain an exhaustive mechanistic scenario we have completed the investigation of the reaction mechanism for **MODEL 1** following the favored reaction channel originating from **m0-*ReRe-cis***. A schematic representation of intermediates and transition states that feature our proposed mechanism is reported in Figures 5 and 6, while the corresponding energy profile is depicted in Figure 4B.

The formation of the C1-C2 bond is completed in the **m1** intermediates that are characterized by the newly formed tetrahydrocarbazolyl skeleton (the **m1** energy levels are reported in Figure 4A). In **m1** the pyrrole ring has lost its aromatic character and bears now a positive charge formally located on C5. Although a new σ C-C bond has been formed, the loss of aromatic character determines an overall destabilization of **m1** with respect to the starting complex. Three new stereocenters are generated in **m1**: C1, C2 and C3. The configuration at C1 is crucial because it determines the position of the H3 proton that will be abstracted in the subsequent re-aromatization step. Depending on its position (corresponding to the existence of two possible stereoisomers), H3 can be facing the allylic hydroxyl (O3H2) or the triflate ion. Importantly, C2 is the only stereocenter that will be maintained during the whole reaction course: thus, the first **m0** → **m1** step determines the stereochemical outcome of the process.

The energetic order of all possible **m1** isomers (Figure 4A) replicates that of the corresponding transition states. The most stable **m1** structure (depicted in Figure 5) is **m1-*ReRe-cis*** which originates from the most stable transition state **ts1-*ReRe-cis***. As one can expect on the basis of the Hammond postulate, being the first reaction step endothermic, **ts1** and **m1** have very similar structural features. Inspection of the **m1-*ReRe-cis*** structure shows that the six-membered ring is complete, even if the C1-C2 bond is slightly longer (1.60 Å) than a normal C-C σ bond. The C2···Au1 interaction has become negligible (C2-Au1 = 3.05 Å) and Au1 is definitely σ-bonded to C3 (Au-C3 = 2.13 Å). Interestingly, in addition to the persisting interaction between the triflate group, the indole ring and the allylic hydroxyl O3H2, a strong hydrogen bond of this group with H3 can be observed (O3···H3(C1) = 2.11 Å). This interaction anticipates the hydrogen abstraction occurring in the next step.

The next two most stable **m1** isomers are **m1-*ReRe-trans*** and **m1-*SiSi-cis***. These minima originate from **ts1-*ReRe-trans*** and **ts1-*SiSi-cis***, respectively i.e. the second and third most stable transition structures. Every other **m1** structure is much higher in energy, confirming that the corresponding reaction channels cannot be competitive. Inspection of the structural features of these intermediates suggests that their instability could be due to unfavorable steric interactions between the phenyl rings of the phosphine ligands and the groups directly involved in the reaction (triflate and allylic hydroxyl).

Second step: proton transfer and rearomatization. In the second step (transition state **ts2**) a proton (H3) is transferred from C1 to the hydroxylic O3 oxygen, affording the intermediate **m2** where the indole aromatic character is re-established. The intrinsic energy barrier for the transformation **m1-*ReRe-cis*** → **ts2** → **m2** is 7.7 kcal mol^{-1}. The proton transfer, favored by the relative position of C1 and O3 which are facing each other in the **m1-*ReRe-cis*** complex, is assisted by the negatively charged triflate ion which, acting as a Lewis base, enhances the basicity of the O3 oxygen through a strong H2···O2 hydrogen-bond (H2···O2 = 1.65 Å). The migrating proton is approximately half-way between C1 and O3 (C1-H3 and O3-H3 ≈ 1.32 Å): this distance is rather large but avoids destabilizing geometrical distortions in the six-member ring-like structure C1-C2-C3-C4-O3-H3.

Since **ts2** is 2.0 kcal mol^{-1} higher than **ts1**, it is responsible for the overall reaction-rate (rate-determining step of the process).

Thus, before discarding the reaction path originating from the most stable isomer **m0-*SiSi-cis***, it is important to check even in that case the energy of **ts2**. We found that this transition state along the ***SiSi-cis*** pathway lies 5.2 kcal mol^{-1} higher. Thus, the ***SiSi-cis*** path is very unlikely and can be definitely ruled out. This result clearly indicates that the favored path is ***ReRe-cis***, which leads to configuration R at C2 in agreement with the experimental evidence.

The resulting **m2** intermediate is characterized by the restored aromatic indole system and the presence of two stereocenters C2 and C3, while C1, after deprotonation, is now an sp^2 hybridized carbon. The positively charged water molecule is bonded to C4 (O3-C4 distance = 1.55 Å) and forms two quite strong hydrogen bonds: one with the indole nitrogen (N···H3 = 1.73 Å) and the other (even stronger) with one of the triflate oxygen atoms (H2···O2 = 1.47 Å, H2-O3 = 1.05 Å), which outlines once again the crucial role of the triflate ion in stabilizing the positive charge now formally located on the O3 atom. The aromatic character of the indole ring mainly determines the high stability of **m2** (1.3 kcal mol^{-1} below **m0-*ReRe-cis***). Certainly the strong interactions involving the triflate ion provide non-negligible contributions to this stability.

Third step: deauration process. In the following third step (**m2 → ts3 → m3**, see Figure 6) we observe the cleavage of the O3-C4 bond and the consequent release of the water molecule (C4···O3 distance = 1.83 Å in **ts3**). The triflate counterion was found to assist the displacement of the water molecule by the persisting strong H2···O2 hydrogen bond (H2···O2 distance = 1.61 Å in **ts3**). This transformation is very fast, (the intrinsic activation barrier being only 1.6 kcal mol^{-1}) and leads to a very stable structure **m3** (14.3 kcal mol^{-1} below the initial reactants). In **m3** the C3-C4 double bond is almost re-established (C3-C4 = 1.38 Å) and the gold atom Au1, where the positive charge is now formally located, is again characterized by an η^2 interaction with the newly formed C3-C4 double bond (C3-Au1 = 2.31 Å and C4-Au1 = 2.40 Å). After displacement, the water molecule is now far away from the C3-C4 moiety (C4···O3 distance = 3.30 Å), but maintains a strong interaction with the negatively charged triflate ion (H2···O2 distance = 1.82 Å).

Fourth step: restoring of the catalytic species. In this last step (**m3 → ts4 → m4**) the bimetallic gold catalyst is restored. Since both **ts4** and **m4** (see Figure 6) are below the starting reactants (-3.5 and -8.8 kcal mol^{-1}, respectively) and the intrinsic activation barrier is 10.8 kcal mol^{-1}, this step must be rather fast indicating an effective catalytic cycle. The mechanism bringing back the catalytic species outlines once again the crucial role of the triflate counterion. In **ts4**, the gold atom Au1 moves from the C3-C4 double bond toward the triflate group: the Au1···O4 distance significantly decreases (2.33 Å) while the distances between the gold atom and C3 and C4 increase (Au1···C3 = 2.78 Å and Au1···C4 = 2.96 Å). Thus, the triflate ion gradually replaces the C3-C4 double bond as a ligand. In the final resulting complex **m4** the bimetallic catalytic complex is definitely re-established (Au1···C3 = 6.32 Å and Au1···C4 = 6.00 Å) and the product is released. The hydrogen-bond of the water molecule to triflate is maintained (O2-H2 = 2.00 Å) while that involving the indole ring becomes weaker (H1-O1 = 2.04 Å).

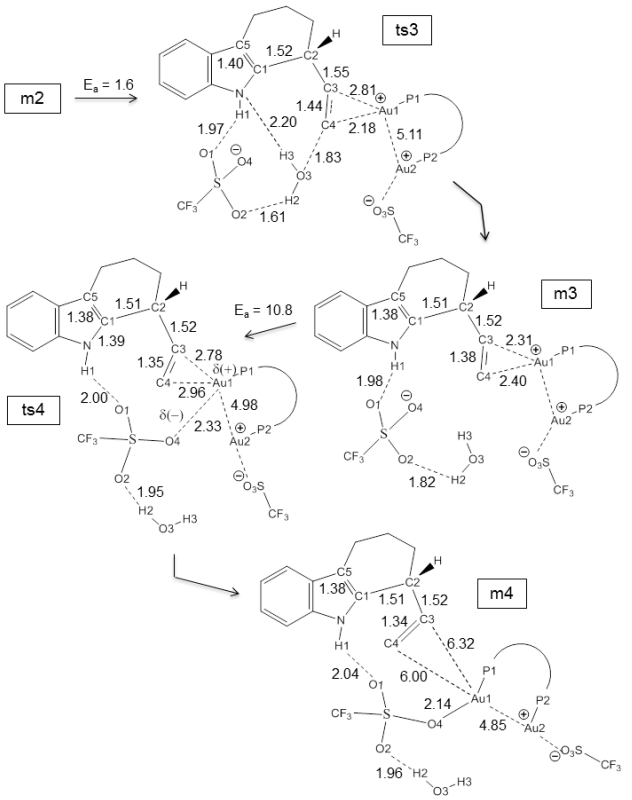

Figure 6. Two-dimensional representations of the critical points **ts3**, **m3**, **ts4** and **m4** located along the reaction path originating from **m0-*ReRe-cis*** (bond lengths are in Ångstroms).

Alternative mechanism: carboauration at the C3 position of the indole. In principle, the initial nucleophilic attack of the adjacent C3 indole carbon atom (C5 in our numbering scheme) on the [Au(I)]-activated olefin should also be considered. As a matter of fact, even C3-substitued indoles have been found to react regioselectively at the more nucleophilic C3 position.[14b,24,25]

Scheme 4. Exploring the initial C(3)-nucleophilic attack of the indole core on the allylic alcohol group.

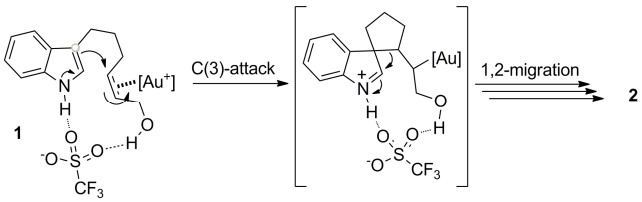

Following this hypothesis (pictorially represented in Scheme 4), the initial carbonauration of the C-C double bond *via* the nucleophilic attack of the carbon C5 was also investigated. This reaction path would lead to the formation of a spiro-compound featuring the new C2-C5 and C3-Au1 bonds. Even in this case, either the *Re* or *Si* face of carbon C5 can be in-

volved in the nucleophilic attack. However, since for a given orientation of the indole ring the C5 *Re* face corresponds to the C1 *Re* face, we can directly compare the transition structures leading to the 5- and 6-member cycles. We have located four possible transition states (denoted as **ts1'**) for this alternative nucleophilic attack. The corresponding energy values relative to the most stable transition state yielding the 6-member cycle (**ts1-*ReRe-cis***), are reported in Table 2. Interestingly, even if the intrinsic activation barriers are of the same order of magnitude as those previously computed, all these new structures are significantly higher in energy than the transition states leading to the 6-member ring. An additional calculation shows that the 5-member cycle intermediate **m1'** (originating from **ts1'-*ReRe-cis***), lies 5.6 kcal mol^{-1} above the most stable 6-member cycle intermediate **m1-*ReRe-cis***. Hence, these alternative reaction channels cannot effectively compete with those leading to the formation of the 6-member cycle.

TABLE 2. Energies (kcal mol^{-1}) of the transition states **ts1'** affording a 5-member cycle. The values are relative to the most stable transition state (**ts1-*ReRe-cis***) affording the 6-member cycle. Intrinsic activation barriers are reported in parenthesis.

ts1' transition states	C2-C3 configuration	
C2 *Re*	*cis*	*trans*
ts1'-*SiRe*	13.1 (17.1)	11.8 (18.1)
ts1'-*ReRe*	2.9 (12.4)	/
C2 *Si*	*cis*	*trans*
ts1'-*SiSi*	7.5 (17.0)	/

The large model system: MODEL 2. The results obtained for **MODEL 1** indicate that the two most likely reaction channels are those originating from **m0-*ReRe-cis*** and **m0-*ReRe-trans***, that involve the same indole and alkene faces but are associated with opposite configurations of the C-C double bond. This result correctly predicts the experimental enantioselectivity for the *cis* isomer. However, even if the reaction on the *trans* species is predicted to be slower (as outlined in the previous section), this finding does not explain the total inability (experimentally observed) of the *trans*-alcohol (*E*)-**1a** to afford the ring closure. This discrepancy between theory and experiment suggested that **MODEL 1** could be an oversimplification of the real system and, thus, was unable to describe properly the stereo-electronic environment generated by the chiral ligand DTBM-MeO-biphep.

To evaluate the effect of the phenyl ring substituents on the reaction profile, we have recomputed the most important critical points using the larger model-system **MODEL 2** that coincides with the real system. In this case, the four phenyl rings (two for each phosphine group), that are not bridging the phosphorous atoms bear a *tert*-butyl group in the two *meta*-positions and one OMe group in the *para*-position. Obviously these four cumbersome rings increase the phosphine steric hindrance: in particular, since at least one phenyl ring is close to the reaction center, in principle they could significantly affect the relative stability of the various critical points. The results of the computations on **MODEL 2** (summarized in Figure 7) show that all the starting reactants, with the exception of **m0-*ReRe-trans***, are very close in energy. This is probably due to the quite large distance between the indole group and the sterically hindered phosphines so that different steric patterns cannot lead to different stabilities. The situation changes in the transition state structures, where the indole approaches the C2-C3 double bond linked to Au1 and consequently the cumbersome ligand side-arms.

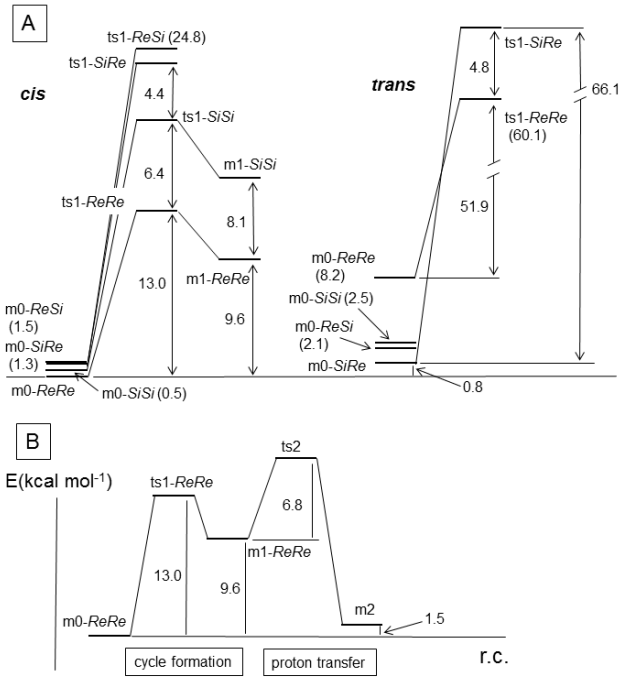

Figure 7. (A) Energies of the *cis* (left side) and *trans* (right side) starting adducts **m0** in the various conformations, the corresponding transition states **ts1** and the resulting intermediates **m1** obtained for **MODEL 2**. Values in parenthesis are relative to **m0-ReRe-cis**. (B) Energy profile for the reaction path originating from **m0-*ReRe- cis.*** Energies in kcal mol^{-1}.

In the case of the *cis* configuration the favored path is again that associated with the most stable **m0-*ReRe-cis*** species (activation energy of 13.0 kcal mol^{-1}). Even if the other *cis* species are rather close in energy, the corresponding activation barriers are significantly higher suggesting that the relating pathways can be ruled out.

To elucidate this point i.e. how much likely are the reaction pathways originating from the other **m0** *cis* structures (in particular that associated with the next most stable transition state **ts1-*SiSi***), we have computed the energy of **m1-*ReRe***, **ts2** and **m2** originating from **m0-*ReRe-cis*** and that of the transition state **ts1-*SiSi-cis*** and intermediate **m1-*SiSi-cis*** (originating from **m0-*SiSi-cis***). The reaction profile **m0-*ReRe-cis*** → **m2** is represented in the lower part of Figure 7. Two important points are evidenced by these computations: (i) since **ts2** is 16.4 kcal mol^{-1} higher than the starting reactants, even for **MODEL 2**, it represents the rate-determining step of the process; (ii) **m1-*SiSi*** (the intermediate along the ***SiSi-cis*** path) lies 8.1 kcal mol^{-1} above **m1-*ReRe*** and 1.3 above **ts2** located

on the ***ReRe-cis*** path. Thus, the ***SiSi-cis*** path (and the two remaining *cis* paths) can be definitely discarded.

To understand why the ***ReRe-cis*** path (leading to configuration *R* at C2) is at a lower energy with respect to the ***SiSi-cis*** path, it is useful to compare the structures of **ts1-*ReRe-cis*** and **ts1-*SiSi-cis***. When the C2 *Si* face (in place of the *Re* face) is involved in the attack, rotations around the C3-C4 and C4-O3 bonds are necessary to activate the H-bond between O3-H2 and the adjacent triflate oxygen. However, this forces one t-Bu group bonded to the P1 non-bridging phenyl ring to move too much closer to the reaction site and the C4 methylene group, thus increasing the steric hindrance and the energy of **ts1-*SiSi-cis***. The structural differences between **ts1-*ReRe-cis* and ts1-*SiSi-cis*** are evidenced in Figures S2 and S3 of the Supplementary Information file.

It is interesting to note that the reaction profile obtained with the more realistic chiral ligand does not change notably with respect to that computed for the smaller model. As found for **MODEL 1**, **m2** is strongly stabilized by the restored aromatic character of the indole moiety and is only 1.5 kcal mol^{-1} above **m0-*ReRe-cis***. A larger activation barrier (13.0 kcal mol^{-1} instead of 9.5 kcal mol^{-1}) has been found for the first step **m0** → **m1**. This is probably due to the more cumbersome phosphine groups, which come closer to the substrate as the reaction proceeds. For the same reason, the first intermediate **m1-*ReRe*** lies 9.6 kcal mol^{-1} above the initial reactants (this value was 3.8 kcal mol^{-1} when the smaller model system was employed).

In the case of the *trans* configuration we have computed the two transition states **ts1-*SiRe-trans*** (associated with the most stable *trans* **m0** isomer) and **ts1-*ReRe-trans***, since for **MODEL 1** we found that the energetics of this path was similar to that of the path originating from **m0-*ReRe-cis***. In both cases the two transition states are very high in energy (i.e. 66.9 and 60.1 kcal mol^{-1} above **m0-*ReRe-cis***, respectively) and large activation barriers feature the corresponding reaction channels (66.1 and 51.9 kcal mol^{-1}, respectively). This computational finding accounts for the negligible reactivity *experimentally recorded for the trans species*. Inspection of the structural features of **ts1-*ReRe-cis*** and **ts1-*ReRe-trans*** shows that the key-factor responsible for the high energy of the latter transition state is again the steric hindrance caused by two *t*-Bu groups bonded to the P1 non-bridging phenyl rings and pointing towards the reaction site: in **ts1-*ReRe-trans*** these groups are forced to move rather close to the double bond and the methylene unit (carbon C4) bearing the hydroxyl group.

In summary, the calculations on **MODEL 2** show that, even if the smaller system provided precious information on the general mechanism of this process (in particular the role played by the gold atoms and triflate ions), a complete model-system including the real cumbersome ligand **L1**, is essential to explain the reagent-controlled stereochemistry of these gold-promoted *enantioselective* transformations.

Finally, a validation of the accuracy of our computational treatment in predicting the overall stereochemical profile of the process was ascertained by determining the absolute configuration of 1-vinyl-tetrahydrocarbazoles **2** (which was found to be *R), via* comparison of the optical rotation values of (*R*)-**2a** and (*R*)-**2f** with the known compounds in literature.[14b]

CONCLUSIONS

The mechanism of the enantioselective gold(I)-catalyzed allylic alkylation of indoles with alcohols has been investigated using a combined experimental-computational DFT approach. To this purpose two model-systems **MODEL 1** and **MODEL 2**, differing in the structure of the gold complex **L1**$(AuOTf)_2$, have been used. In the former case the Ar groups not bridging the two P atoms are simple benzene rings while in latter case (corresponding to the real adduct used in the experiment) Ar = 3,5-(*t*-Bu)$_2$-4-OMe-Ph.

The results obtained with the two model-systems can be summarized as follows:

(i) The fully explored reaction surface for **MODEL 1** reveals that the favoured mechanism is a step-wise S_N2' type mechanism based on indole-auration of the C-C double bond (outer-sphere like), re-aromatization of the indole moiety and subsequent β-elimination of [Au(I)]-H_2O.

(ii) The triflate gold counterion has been demonstrated to play a pivotal role several times along the reaction coordinate. First of all this ion exerts a sort of "*folding effect"* which forces the two reactive sites of the starting adduct to move closer adopting the right orientation to react (U-turn-type geometry). This is achieved by means of two rather strong H-bonds involving the indole NH bond, the allylic hydroxyl group and two triflate oxygen atoms. This hypothesis has been confirmed by additional experimental results on modified reacting systems where the above described H-bonds cannot be established. The negatively charged triflate ion plays an additional important role in "assisting" the proton transfer from C1 (C(2) indole position) to the allylic hydroxyl oxygen O3 and, thus, restoring the aromatic character of the pyrrolyl ring (second step of the process, transition state **ts2**). The triflate ion strongly interacts with the hydroxyl hydrogen H2 (H2···O2 = 1.65 Å) and enhances the basicity of the hydroxyl oxygen. The role of the triflate counterion is once again crucial in the third reaction step (**ts3**) where the release of the water molecule (needed to restore a C-C double bond) is helped by the persisting strong hydrogen bond between this ion (oxygen O2) and the water hydrogen H2 (H2···O2 distance = 1.61 Å in **ts3**). All these aspects contribute to make this transformation very fast.

(iii) The low energy barrier that features the transition state corresponding to the formation of the new carbon-carbon bond (**ts1**) can be explained by the electrophilic character of the C2-C3 double bond, enhanced by the interaction with the gold atom and by the pronounced "*folding effect*" found in the transition structure.

(iv) Being **ts2** the highest in energy transition state, the corresponding step (where the aromatic character of the indole ring is restored) determines the overall kinetics and is the rate-determining step of the process.

(v) The new stereocenter at C2 is formed in the first reaction step and is maintained along the whole reaction path. The absolute configuration of this carbon in the final products is *R* in agreement with the experimental finding.

(vi) Even if the simpler model provides a complete mechanistic scenario for these reactions, it does not correctly predict the

influence of the stereochemistry of the reaction partners and the dichotomy in reactivity of the two diastereomeric *Z* and *E* acyclic precursors **1a**. To explain this aspect it is essential to use a larger model corresponding to the real system used in the experiment and including the cumbersome *t*-Bu groups bonded to the non-bridging phenyl groups of the ligand. When the C2-C3 double bond has a *trans* configuration (**ts1-*ReRe-trans***) two of these groups (pointing toward the reaction site) are forced too much close to the double bond and the methylene unit (carbon C4) bearing the hydroxyl group, thus causing a destabilizing steric hindrance. The steric hindrance caused by the cumbersome *t*Bu groups is also responsible for lower energy of the ***ReRe-cis*** path (leading to configuration *R* at C2) compared to the ***SiSi-cis*** path and, thus, for the e.e. experimentally observed.

(vii) The nucleophilic attack of the C3 indole carbon atom (C5 in our numbering scheme) on the [Au(I)]-activated olefin (formation of a 5-member cyclic intermediate) seems disfavored with respect to the attack of the C2 indole carbon (C1 in our model-system).

COMPUTATIONAL DETAILS

All the reported DFT computations have been carried out with the Gaussian 09[26] series of programs using the B3LYP[27] functional that has been demonstrated to provide a reliable description of systems involving metal atoms and hydrogen bond interactions.[28] According to a locally dense basis set (LDBS)[29] approach, the model-system has been partitioned into different regions, which were assigned basis sets of different accuracy. For **MODEL 1** all atoms, except the gold atoms, have been described by the DZVP basis,[30] which is a Local Spin Density (LSD)-optimized basis set of double-zeta quality including polarization functions. For the two metal atoms we used the LANL2DZ basis set.[31] For **MODEL 2** we have maintained the same accuracy level of **MODEL 1** except for the methyl groups added in the larger model. Thus, the carbon and hydrogen atoms of the methyl belonging to *t*-Bu and OMe have been described by the simple STO-3G basis, but we have used the DZVP basis for oxygen in OMe and the central carbon in *t*-Bu. We have performed frequency computations to determine the nature of the various critical points.

ASSOCIATED CONTENT

Supporting Information. Experimental methods, compound characterizations and detailed computational results. This material is available free of charge via the Internet at http://pubs.acs.org.

AUTHOR INFORMATION

Corresponding Authors

*E-mail: gianpiero.miscione@unibo.it (G.M.), marco.bandini@unibo.it (M.B.).

ACKNOWLEDMENTS

Acknowledgment is made to Progetto FIRB-2008 "Futuro in Ricerca" *Innovative sustainable synthetic methodologies for C-H activation processes*, Progetto PRIN-2009 "*Progettazione e sviluppo di sistemi catalitici innovativi*" (MIUR, Rome) and Alma Mater Studiorum - Università di Bologna.

ABBREVIATIONS

dppm: 1,1-bis(diphenylphosphino)methane; DTBM: 3,5-tBu$_2$-4-OMe; ee: enantiomeric excess; LA: Lewis acid; MeObiphep: 2,2'-bis(diphenylphosphino)-6,6'-dimethoxy-1,1'-biphenyl; nr: no reaction; NTf_2: bis(trifluoromethylsulfonyl)amide; OPBN: *p*-nitrobenzoate; OTf: trifluoromethanesulfonate; OTs: *p*-toluenesulfonate; THBCs: tetrahydro-β-carbolines.

REFERENCES

(1) (a) R. A. Widenhoefer, *Chem. Eur. J.* **2008**, *14*, 5382-5391. (b) D. J. Gorin, B. D. Sherry, F. D. Toste, *Chem. Rev.* **2008**, *108*, 3351-3378. (c) N. Bongers, N. Krause, *Angew. Chem. Int. Ed.* **2008**, *47*, 2178-2181. (d) S. Sengupta, X. Shi, *Chem. Cat. Chem.* **2010**, *2*, 609-619. (e) A. S. K. Hashmi, C. Hubbert, *Angew. Chem. Int. Ed.* **2010**, *49*, 1010-1012. (f) A. Pradal, P. Y. Toullec, V. Michelet, *Synthesis* **2011**, 1501-1514.

(2) For general reviews on gold-catalyzed organic transformations see: (a) A. S. K. Hashmi, *Angew. Chem. In. Ed.* **2005**, *44*, 6990-6993. (b) A. S. K. Hashmi, G. J. Hutchings, *Angew. Chem. Int. Ed.* **2006**, *45*, 7896-7936. (c) D. J. Gorin, F. D. Toste, *Nature* **2007**, *446*, 395-403. (d) A. S. K. Hashmi, *Chem. Rev.* **2007**, *107*, 3180-3211. (e) A. Fürstner, O. D. Davies, *Angew. Chem. Int. Ed.* **2007**, *46*, 4310-4317. (f) Z. Li, C. Brouwer, C. He, *Chem. Rev.* **2008**, *108*, 3239-3265. (g) E. Jiménez-Núñez, A. M. Echavarren, *Chem. Rev.* **2008**, *108*, 3326-3350. (h) H. C. Shen, *Tetrahedron* **2008**, *64*, 3885-3903. (i) R. Skouta, C.-J. Li, *Tetrahedron* **2008**, *64*, 4917-4938. (j) A. Arcadi, *Chem. Rev.* **2008**, *108*, 3266-3325. (k) P. Belmont, E. Parker, *Eur. J. Org. Chem.* **2009**, 6075-6089. (l) N. D. Shapiro, F. D. Toste, *Synlett*, **2010**, 675-691. (m) A. Corma, A. Leyva-Pérez, M. J. Sabater, *Chem. Rev.* **2011**, *111*, 1657-1712. (n) T. de Haro, C. Nevado, *Synthesis*, **2011**, 2530-2539. (p) M. Bandini, *Chem. Soc. Rev.* **2011**, *40*, 1358-1367. (q) T. C. Boorman, I. Larrosa, *Chem. Soc. Rev.* **2011**, *40*, 1910-1925.

(3) L.-I. Rodríguez, T. Roth, J. Lloret Fillol, H. Wadepohl, L. H. Gade, *Chem. Eur. J.* **2012**, *18*, 3721-3728.

(4) For a general review see: (a) D. Benitez, N. D. Shapiro, E. Tkatchouk, Y. Wang, W. A. Goddard, F. D. Toste, *Nat. Chem.* **2009**, *1*, 482. (b) A. S. K. Hashmi, *Angew. Chem. Int. Ed.* **2010**, *49*, 5232-5241. For a selection of articles see: (c) G. Seidel, R. Mynott, A. Fürstner, *Angew. Chem. Int. Ed.* **2009**, *48*, 2510-2513. (d) D. Weber, M. A. Tarselli, M. R. Gagné, *Angew. Chem. Int. Ed.* **2009**, *48*, 5733-5736. (e) R. S. Paton, F. Maseras, *Org. Lett.* **2009**, *11*, 2237-2240. (f) Z. J. Wang, D. Benitez, E. Tkatchouk, W. A. Goddard, F. D. Toste, *J. Am. Chem. Soc.* **2010**, *132*, 13064-13071. (g) R. L. LaLonde, W. E. Brenzovich, D. Benitez, E. Tkatchouk, K. Kelly, W. A. Goddard, F. D. Toste, *Chem. Sci.* **2010**, *1*, 226-233. (h) P. Pérez-Galán, E. Herrero-Gómez, D. T. Hog, N. J. A. Martin, F. Maseras, A. M. Echavarren, *Chem. Sci.* **2011**, *2*, 141-149. (i) P. Nun, S. Gaillard, A. Poater, L. Cavallo, S. P. Nolan, *Org. Biomol. Chem.* **2011**, *9*, 101-104. (j) A. S. K. Hashmi, M. Pernpointner, M. M. Hansmann, *Faraday Discussion*, **2011**, *152*, 179-184. (k) R. Döpp, C. Lothschütz, T. Wurm, M. Pernpointner, S. Keller, F. Rominger, A. S. K. Hashmi, *Organometallics*, **2011**, *30*, 5894-8903. (l) E. L. Noey, X. Wang, K. N. Houk, *J. Org. Chem.* **2011**, *76*, 3477-3483. (m) O. A. Egorova, H. Seo, Y. Kim, D. Moon, Y. M. Rhee, K. H. Ahn, *Angew. Chem. Int. Ed.* **2011**, *50*, 11446-11450. (n) E. L. Noey, Y. Luo, L. Zhang, K. N. Houk, *J. Am.* Chem. Soc. **2012**, *134*, 1078-1084. (p) J. E. Heckler, M. Zeller, A. D. Hunter, T. G. Gray, *Angew. Chem. Int. Ed.* **2012**, *51*, 5924-5928.

(5) Chiral monometallic gold complexes are also emerging as valuable alternative see: 4a, (a) H. Teller, S. Flügge, R. Goddard, A. Fürstner, *Angew. Chem. Int. Ed.* **2010**, *49*, 1949-1953. (b) H. Teller, A. Fürstner, *Chem. Eur. J.* **2011**, *17*, 7764-7767.

(6) (a) H. Schmidbaur, A. Schier, *Z. Naturforsch.* **2011**, *66b*, 329-350. (b) D. Wang, R. Cai, S. Sharma, J. Jirak, S. K. Thummanapelli, N. G. Akhmedov, H. Zhang, X. Liu, J. L. Petersen, X. Shi, *J. Am. Chem. Soc.* **2011**, *134*, 9012-9019.

(7) A. L. Pérez, A. Corma, *Angew. Chem. Int. Ed.* **2012**, *51*, 614-635.

(8) (a) M. J. Johansson, D. J. Gorin, S. T. Staben, F. D. Toste, *J. Am. Chem. Soc.* **2005**, *127*, 18002-18003. (b) G. L. Hamilton, E. J. Kang, M. Mba, F. D. Toste, *Scienze*, **2007**, *317*, 496-499.

(9) D. Zuccaccia, L. Belpassi, F. Tarantelli, A. Macchioni, *J. Am. Chem. Soc.* **2009**, *131*, 3170-3171, and references therein.

(10) (a) M. Bandini, A. Eichholzer, P. Kotrusz, M. Tragni, S. Troisi, A. Umani-Ronchi, *Adv. Synth. Catal.* **2009**, *351*, 319-324. (b) M. Bandini, M. Tragni, A. Umani-Ronchi, *Adv. Synth. Catal.* **2009**, *351*, 2521-2524. (c) M. Bandini, A. Eichholzer, A. Gualandi, T. Quinto, D. Savoia, *Chem. Cat. Com.* **2010**, *2*, 661-665. (d) M. Chiarucci, M. Locritani, G. Cera, M. Bandini, *Beilstein J. Org. Chem.* **2011**, *7*, 1198-1204. (e) G. Cera, S. Piscitelli, M. Chiarucci, G. Fabrizi, A. Goggiamani, R. S. Ramón, S. P. Nolan, M. Bandini, *Angew. Chem. Int. Ed.* **2012**, *51*, 9891-9895.

(11) For a review see: (a) M. Bandini, *Angew. Chem. Int. Ed.* **2011**, *50*, 994-995. (b) M. Bandini, G. Cera, M. Chiarucci, *Synthesis*, **2012**, 504-512.

(12) (a) M. Bandini, A. Eichholzer, *Angew. Chem. Int. Ed.* **2009**, *48*, 9533-9537. (b) M. Bandini, A. Gualandi, M. Monari, A. Romaniello, D. Savoia, M. Tragni, *J. Organomet. Chem.* **2011**, *696*, 338-347. (c) M. Bandini, M. monari, A. Romaniello, M. Tragni, *Chem. Eur. J.* **2010**, *16*, 14272-14277.

(13) (a) M. Somei, F. Yamada, *Nat. Prod. Rep.* **2005**, *22*, 73-103. (b) G. R. Humphrey, J. T. Kuethe, *Chem. Rev.* **2006**, *106*, 2875-2911. (c) TB. M. rost, M. K. Brennan, *Synthesis*, **2009**, 3003-3025. (d) A. J. Kochanowska-Karamyan, M. T. Hamann, *Chem. Rev.* **2010**, *110*, 4489-4497.

(14) Recent catalytic enantioselective synthesis of tetrahydrocarbazoles: (a) X.-Y. Zhu, X.-L. An, C.-F. Li, F.-G. Zhang, Q.-L. Hua, J.-R. Chen, W.-J. Xiao, *Chem. Cat. Chem.* **2011**, *3*, 679-683. (b) Q.-F. Wu, C. Zheng, S.-L. You, *Angew. Chem. Int. Ed.* **2012**, 51, 1680-1683.

(15) For some leading examples see: (a) C. Liu, R. A. Widenhoefer, *Org. Lett.* **2007**, *9*, 1935-1938. (b) Ö. Aksin, N. Krause, *Adv. Synth. Catal.* **2008**, *350*, 1106-1112. (c) A. Aponick, C.-Y. Li, B. Biannic, *Org. Lett.* **2008**, *10*, 669-671. (d) F. Volz, S. H. Wadman, A. Hoffmann-Röder, N. Krause, *Tetrahedron*, **2009**, *65*, 1902-1910. (e) P. Mukherjee, R. A. Widenhoefer, *Org. Lett.* **2010**, *12*, 1184-1187. (f) A. Aponick, B. Biannic, *Org. Lett.* **2011**, *13*, 1330-1334. (g) P. Mukherjee, R. A. Widenhoefer, *Org. Lett.* **2011**, *13*, 1334-1337. (h) S. R. K. Minkler, B. H. Lipshutz, N. Krause, *Angew. Chem. Int. Ed.* **2011**, *50*, 7820-7823. (i) P. Mukherjee, R. A. Widenhoefer, *Angew. Chem. Int. Ed.* **2012**, *51*, 1434-1436.

(16) *Modern Gold Catalyzed Synthesis*, (A. S. K. Hashmi, F. D. Toste, Eds.) Wiley-VCH, Weinheim, **2012**.

(17) B. Biannic, A. Aponick, *Eur. J. Org. Chem.* **2011**, 6821-6824.

(18) (a) M. Georgy, V. Boucard, J.-M. Campagne, *J. Am. Chem. Soc.* **2005**, *127*, 14180-14181. (b) M. Georgy, V. Boucard, O. Debleds, C. Dal Zotto b, J.-M. Campagne, *Tetrahedron*, **2009**, *65*, 1758-1766. (c) O. Debleds, E. Gayon, E. Vrancken, J.-M. Campagne, *Beilstein J. Org. Chem.* **2011**, *7*, 866-877.

(19) For a recent review: N. T. Patil, *Chem. Asian J.* **2012**, *7*, 2186-2194.

(20) R. L. LaLonde, B. D. Sherry, E. J. Kang, F. D. Toste, *J. Am. Chem. Soc.* **2007**, *129*, 2452-2453.

(21) For representative examples see: (a) K. Aikawa, M. Kojima, K. Mikami, *Angew. Chem. Int. Ed.* **2009**, *48*, 6073-6077. (b) R. L. Lalonde, J. Z. Wang, M. Mba, A. D. Lackner, F. D. Toste, *Angew. Chem. Int. Ed.* **2010**, *49*, 598-601. (c) K. Aikawa, M. Kojima, K. Mikami, *Adv. Synth. Catal.* **2010**, *352*, 3131-3135. (d) C. H. Cheon, O. Kanno, F. D. Toste, *J. Am. Chem. Soc.* **2010**, *133*, 13248-13251.

(22) (a) R. M. Beesley, C. K. Ingold, J. F. Thorpe, *J. Chem. Soc.*, **1915**, *107*, 1080-1106. (b) C. K. Ingold, *J. Chem. Soc.*, **1921**, *119*, 305-329. (c) C. K. Ingold, S. Sako, J. F. Thorpe, *J. Chem. Soc.*, **1922**, 1117-1198.

(23) H. Schmidbaur, A. Schier, *Chem. Soc. Rev.* **2012**, *41*, 370-412, and references therein.

(24) For general reviews: (a) E. D. Cox, J. M. Cook, *Chem. Rev.* **1995**, *95*, 1797-1842. (b) M. Bandini, A. Eichholzer, *Angew. Chem. Int. Ed.* **2009**, *48*, 9608-9644. (c) B. M. Trost, M. K. Brennan, *Synthesis*, **2009**, 3003-3025.

(25) For a selection of recent examples of stereo- and regioselective functionalization of C3-substituted indoles see: (a) B. M. Trost, J. Quancard *J. Am. Chem. Soc.* **2006**, *128*, 6314-6315. (b) B. M. Trost, M. K. Brennan *Synthesis*, **2009**, 3003-3025. (c) Q.-F. Wu, H. He, W.-B. Liu, S.-L. You, *J. Am. Chem. Soc.* **2010**, *132*, 11418-11419. (d) Q. Cai, C. Zheng, J.-W. Zhang, S.-L. You, *Angew. Chem. Int. Ed.* **2011**, *50*, 8665-8669. (e) B. Jones, B. Simmons, A. Mastracchio, D. W. C. MacMillan, *Nature*, **2011**, *475*, 183-188, and references therein. (f) G. Cera, M. Chiarucci, A. Mazzanti, M. Mancinelli, M. Bandini, *Org. Lett.* **2012**, *14*, 1350-1353.

(26) Gaussian 09, Revision A.02, M. J. Frisch, G. W. Trucks, H. B. Schlegel, G. E. Scuseria, M. A. Robb, J. R. Cheeseman, G. Scalmani, V. Barone, B. Mennucci, G. A. Petersson, H. Nakatsuji, M. Caricato, X. Li, H. P. Hratchian, A. F. Izmaylov, J. Bloino, G. Zheng, J. L. Sonnenberg, M. Hada, M. Ehara, K. Toyota, R. Fukuda, J. Hasegawa, M. Ishida, T. Nakajima, Y. Honda, O. Kitao, H. Nakai, T. Vreven, J. A. Montgomery, Jr., J. E. Peralta, F. Ogliaro, M. Bearpark, J. J. Heyd, E. Brothers, K. N. Kudin, V. N. Staroverov, R. Kobayashi, J. Normand, K. Raghavachari, A. Rendell, J. C. Burant, S. S. Iyengar, J. Tomasi, M. Cossi, N. Rega, J. M. Millam, M. Klene, J. E. Knox, J. B. Cross, V. Bakken, C. Adamo, J. Jaramillo, R. Gomperts, R. E. Stratmann, O. Yazyev, A. J. Austin, R. Cammi, C. Pomelli, J. W. Ochterski, R. L. Martin, K. Morokuma, V. G. Zakrzewski, G. A. Voth, P. Salvador, J. J. Dannenberg, S. Dapprich, A. D. Daniels, O. Farkas, J. B. Foresman, J. V. Ortiz, J. Cioslowski, D. J. Fox, Gaussian, Inc., Wallingford CT, 2009.

(27) (a) C. Lee, W.T. Yang, R.G. Parr, *Phys Rev B: Condens Matter* **1988**;*37*, 785-789. (b) A.D. Becke. *J Chem Phys* **1993**, *98*, 5648-5652

(28) (a) L. Fan, T. Ziegler, *J. Am. Chem. Soc.* **1992**, *114*, 10890-10897. (b) A. Bottoni, A. Perez Higueruelo, G. P. Miscione, *J. Am. Chem. Soc.* **2002**, *124*, 5506-5513. (c) A. Bottoni, C. Z. Lanza, G. P. Miscione, D. Spinelli, *J. Am. Chem. Soc.* **2004**, *126*, 1542-1550. (d) R. D. Bach, C. Thorpe, O. Dmitrenko, *J. Phys. Chem. B* **2002**, *106*, 4325-4335.

(29) G. A. DiLabio, D. A. Pratt, J. S. Wright, *Chem. Phys. Lett.* **1998**, *297*, 181-186.

(30) N. Godbout, D. R. Salahub, J. Andzelm, E. Wimmer, *Can. J. Chem.* **1992**, *70*, 560-571.

(31) (a) P. J. Hay, W. R. Wadt, *J. Chem. Phys.* **1985**, *82*, 270-283. (b) P. J. Hay, W. R. Wadt, *J. Chem. Phys.* **1985**, *82*, 284-299. (c) P. J. Hay, W. R. Wadt, *J. Chem. Phys.* **1985**, *82*, 299C.

TOC

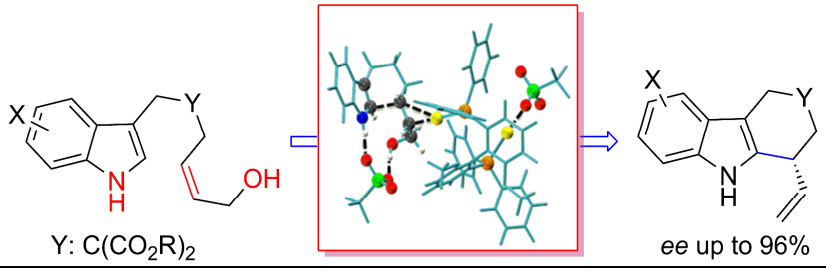

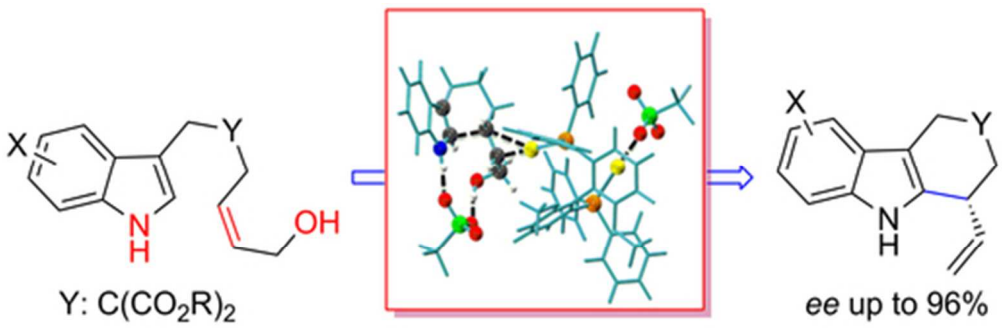

43x14mm (300 x 300 DPI)